PROTEINS: Structure, Function, and Bioinformatics 67:000–000 (2007)

COMBINE Analysis of the Specificity of Binding of Ras Proteins to their Effectors

Sanja Tomić,[1*] Branimir Bertoša,[1] Ting Wang,[2] and Rebecca C. Wade[2]
[1]*Ruđer Bošković Institute, Bijenička 54, Zagreb, Croatia*
[2]*Molecular and Cellular Modeling Group, EML Research gGmbH, Schloss-Wolfsbrunnenweg 33, Heidelberg, Germany*

ABSTRACT **The small guanosine triphosphate (GTP)-binding proteins of the Ras family are involved in many cellular pathways leading to cell growth, differentiation, and apoptosis. Understanding the interaction of Ras with other proteins is of importance not only for studying signalling mechanisms but also, because of their medical relevance as targets, for anticancer therapy. To study their selectivity and specificity, which are essential to their signal transfer function, we performed COMparative BINding Energy (COMBINE) analysis for 122 different wild-type and mutant complexes between the Ras proteins, Ras and Rap, and their effectors, Raf and RalGDS. The COMBINE models highlighted the amino acid residues responsible for subtle differences in binding of the same effector to the two different Ras proteins, as well as more significant differences in the binding of the two different effectors (RalGDS and Raf) to Ras. The study revealed that E37, D38, and D57 in Ras are nonspecific hot spots at its effector interface, important for stabilization of both the RalGDS–Ras and Raf–Ras complexes. The electrostatic interaction between a GTP analogue and the effector, either Raf or RalGDS, also stabilizes these complexes. The Raf–Ras complexes are specifically stabilized by S39, Y40, and D54, and RalGDS–Ras complexes by E31 and D33. Binding of a small molecule in the vicinity of one of these groups of amino acid residues could increase discrimination between the Raf–Ras and RalGDS–Ras complexes. Despite the different size of the RalGDS–Ras and Raf–Ras complexes, we succeeded in building COMBINE models for one type of complex that were also predictive for the other type of protein complex. Further, using system-specific models trained with only five complexes selected according to the results of principal component analysis, we were able to predict binding affinities for the other mutants of the particular Ras-effector complex. As the COMBINE analysis method is able to explicitly reveal the amino acid residues that have most influence on binding affinity, it is a valuable aid for protein design. Proteins 2007;67:000–000.** © 2007 Wiley-Liss, Inc.

Key words: Ras; RalGDS; Raf; Rap; mutation; binding affinity; binding specificity; Poisson–Boltzmann electrostatics; hot spots; quantitative structure-activity relationship

INTRODUCTION

Signal transfer in biological systems depends on protein–protein interactions. Protein mutations and changes in environment can abolish signaling pathways within cells, leading to severe damage and disease. The first identified and the most studied role of Ras family members is in cell transformation. The small guanosine triphosphate (GTP)-binding proteins of the Ras family are involved in many cellular pathways leading to cell growth, differentiation, and apoptosis.[1] Regulatory proteins, guanine nucleotide exchange factors (GEFs), and GTPase activating proteins (GAPs) turn Ras, and Ras-related GTP-binding proteins, on and off.[2] In the active, *on* conformation, Ras interacts with the effector Raf, a Ser/Thr specific protein kinase that is an immediate downstream target of Ras in the mitogen-activating protein kinase pathway (MAPK).[3] Certain mutations in Ras destroy this switch function. In the mutated Ras protein, the hydrolysis of GTP to GDP is not possible and Ras remains in its active *on* conformation. In this way, the signal transduction is amplified and cells grow and divide uncontrolled. The mutated Ras, as well as other proteins involved in Ras signal transduction, are frequently found in diverse human tumors.[3–5] Mutations in

Abbreviations: COMBINE, COMparative BINding Energy; GDP, guanosine diphosphate; GNP, guanosine 5′-(β,γ-imido)triphosphate (GppNHp); GTP, guanosine triphosphate; PC, principal components; PLS, partial least square; QSAR, quantitative structure activity relationship; Raf, Raf kinase; RalGDS, guanine nucleotide dissociation stimulator of the small GTPase Ral; Rap, Rap1A—member of the Ras small G protein superfamily; Ras, protein product of human Ha-Ras; RBD, Ras binding domain of effector molecule; RMSD, root mean square deviation.

Complexes are named by the mutation made in the effector, either RalGDS or Raf followed by the mutation made in Ras, WT indicates wild-type.

The Supplementary Material referred to in this article can be found at http://www.interscience.wiley.com/jpages/0887-3585/suppmat/

Grant sponsor: Klaus Tschira Foundation; Grant sponsor: German-Croatian bilateral WTZ project; Grant number: HRV01/010

Ting Wang's Current address is UC Davis Genome Center, 431 East Health Science Drive, University of California, Davis, CA 95616-8816.

**Correspondence to:* Sanja Tomić, Ruđer Bošković Institute, Bijenička 54, Zagreb, Croatia. E-mail: sanja.tomic@irb.hr

Received 4 August 2006; Revised 10 October 2006; Accepted 6 November 2006

Published online 00 Month 2007 in Wiley InterScience (www.interscience.wiley.com). DOI: 10.1002/prot.21321

Ras that permanently activate it have been found in about half of all colon cancers and over 95% of pancreatic cancers. Another effector protein that Ras-proteins interact with is Ral guanine nucleotide dissociation stimulator (RalGDS). This interaction regulates Rho/Rac family members that control cytoskeletal rearrangements.[6] There is also experimental evidence that Ras is involved in transcription not only through its binding to Raf, but also through its binding to RalGDS.[7,8] The activation of RalGDS in human cells, rather than Raf or phosphoinositol-3-kinase (PI3K), plays a central role in the Ras-induced oncogenic transformation.[9–11] In this paper, we compare the binding of Ral and Raf to Ras, and Rap, another member of the Ras family.

Members of the Ras family share the same core effector binding region (residues 32–40) differing only by a few different flanking amino acids.[12] From the solved structures of Ras protein–effector complexes,[13–16] it is evident that Ras proteins bind to their effectors by establishing an intermolecular β-sheet consisting of two β-strands from the Ras protein and two β-strands from the effector's Ras binding domain (RBD). All Ras effectors analyzed so far have structurally similar RBDs characterized by a ββαββαβ ubiquitin fold, although the sequence homology in their RBDs is low. Despite the structural similarities of RBDs, Ras proteins bind to different effectors highly specifically. These findings make the study of selectivity and specificity of Ras proteins intriguing.

The availability of crystal and NMR structures of Ras family members[17,18] and their mutants,[19–25] as well as structures of Ras-effector complexes,[13–16] have enabled a number of theoretical studies of the flexibility of proteins, their specificity, and selectivity.[26–32]

Kiel et al.[29] performed an exhaustive mutagenesis analysis of Ras proteins and their effectors by both experimental and theoretical analysis. They made single point interfacial mutants of the Ha-Ras and Rap1A proteins, and their effectors, RalGDS and Raf. Using isothermal titration calorimetry and fluorescence measurements, they determined the thermodynamic binding parameters (binding free energy, enthalpy, and entropy) of Ras proteins to their effectors. Using the FOLD-X energy function, they predicted the binding free energy differences between the mutant complexes. Their assumptions that there are no major conformational changes of the proteins upon single point mutation or during the complex formation seem to hold up for the majority of the complexes studied since they predicted the binding free energy of different mutants with good accuracy. For Ras-RalGDS complexes, the correlation (R) between calculated and experimental ΔG values is 0.88, with a slope of 0.86; for Ras-Raf complexes, the corresponding values are 0.77 and 0.62. Their study revealed differences in the energy landscape for RalGDS and Raf effectors binding to Ras proteins, and similarity in the importance of different types of interactions in the formation of complexes between Ras proteins and their effectors. According to their results, electrostatic interactions and hydrogen-bond formation are favored over hydrophobic interactions.

Gohlke et al.[28] computed the binding free energies for the Ras-Raf and Ras-RalGDS complexes using the molecular mechanics (MM)-generalized Born surface area (GBSA) approach and 5 ns of MD simulation for the unbound proteins, Ras, Raf and RalGDS, and the complexes, Ras-Raf and Ras-RalGDS. On the basis of snapshots extracted from the simulations, they calculated energy and entropy contributions to the binding free energies. They found that overall the electrostatic interactions disfavor protein–protein binding, not only in the case of Ras and RalGDS proteins, whose net charges are of the same sign, but also in the case of Ras and Raf proteins, which have opposite net charges. On the other hand, Muegge et al.,[30] and Sheinerman and Honig,[31] who both studied the interaction between the RBD of Raf and the Ras homologue Rap1A, found that the electrostatic contribution favors protein–protein association. The main difference between the study of Gohlke et al. and that of the other two groups is in the treatment of the structure of the unbound proteins. Gohlke et al.[30] used the structures of unbound proteins found in the PDB (determined by X-ray diffraction), while the other two groups extracted the individual proteins from the structure of their complex and allowed either no[30] or only a limited[31] relaxation of these.

In the present work, we studied the wild type RalGDS-RBD–Ras-GppNHp, RalGDS-RBD–Rap-GppNHp, and Raf-RBD–Ras-GppNHp complexes, as well as their mutant complexes (53, 21, and 45 complexes, respectively). We used a Poisson–Boltzmann continuum model for electrostatics calculations[33] and performed COMparative BINding Energy (COMBINE) analysis[34–36] to derive a system-specific quantitative structure activity relationship (QSAR) model for estimating binding free energy differences. COMBINE analysis is based upon the assumption that the binding free energy (ΔG) can be correlated with a subset of suitably weighted energy components (u_i) determined from the structures of the two proteins in bound and unbound forms.

$$\Delta G = \sum_i w_i u_i + C \tag{1}$$

The contribution of each interaction energy term is represented by its weight, w_i in Eq. (1). The weights are obtained by PLS (partial least squares) analysis using a training set of complexes with experimentally determined binding affinities. The resultant COMBINE model is a system-specific model for binding affinity that, due to the residue-based decomposition, indicates the most important interactions governing binding affinity differences for the complexes studied. The COMBINE model can be used to make predictions of the effects on binding affinity of mutating residues in the complexes. The COMBINE analysis method has proved successful for deriving high quality QSAR models for a variety of protein–ligand complexes including enzyme–inhibitor,[34–40] enzyme–substrate,[41–43] protein–peptide,[44] nuclear receptor–DNA complexes,[45,46] and protein–protein complexes.[47]

This study is based on the crystal structures of the native enzymes from the Ras family as well as the structures of their mutants in complexes with the effector proteins RalGDS and Raf.[13–15] It also makes use of ther-

J_ID: Z7E Customer A_ID: 21321 Cadmus Art: PROT21321 Date: 4-FEBRUARY-07 Stage: I Page: 3

modynamic measurements for these proteins.[29] First, the structures of the 122 Ras-protein–effector complexes with different interfacial mutations were modeled and energy minimized using the structures of the wild-type protein complexes as templates. The intermolecular energy was decomposed on a residue pair basis and the electrostatic contribution to the desolvation free energy was calculated using the finite difference Poisson–Boltzmann equation. Models that correlate the calculated energy terms with the experimental binding free energy were built by training on only a few complexes (five) selected according to the results of PC analysis of each set of Ras-effector mutants and used to predict the binding affinity for the other mutants of these proteins. The standard deviations in the errors of predictions (SDEP)s, $\sqrt{\sum_{i=1}^{Ns}(\Delta G_{exp} - \Delta G_{calc})^2/Ns}$, for the external data sets of Ras-Raf and Ras-RalGDS complexes are 1.07 and 1.06, respectively. Such a good predictive performance of the models derived from training on only a few complexes indicates the applicability of the method for planning experiments to study protein binding specificity. The predictive ability of these models is comparable with the predictions achieved with FoldX. The SDEPs of the FoldX-calculated binding free energies for the single mutants of Ras-RalGDS and Ras-Raf complexes are 0.72 and 0.65, respectively.

METHODS

Molecular Mechanics Modeling

Preparation of mutant complexes

The crystallographic structure of the complex between the Ras binding domain (RBD) of RalGDS with the E31K mutant of Ras,[16] extracted from the Protein Databank (code 1LFD), was used as the template for preparing all mutant complexes. For this purpose, K31 in Ras was mutated back to E. There are two complexes (AB and CD) in the asymmetric unit of the crystal cell with the RMSD of their backbone atoms being 0.68 Å. To increase the robustness of the model, we considered both structures in our calculations. The differences between these two complexes are more pronounced for RalGDS than Ras; the RMSDs between the backbone atoms are 0.60 Å, and 0.36 Å, respectively, and the RMSDs of all heavy atoms are 1.25 Å and 0.95 Å, respectively. For building Ras-Ral mutant complexes for which experimentally measured binding affinity is available,[29] mutations were introduced at 11 Ras residues (Q25, V29, E31, D33, E37, D38, S39, Y40, R41, E62, E63) and 13 RalGDS residues (I14, R16, N23, N25, Y27, K28, S29, K44, D47, K48, H49, D52, E53) (Fig. 1). F1

The RafRBD–Ras complexes were prepared starting from PDB files 1LFD, containing a Ras–RalGDS complex, and 1C1Y.[13] 1C1Y and 1GUA contain the crystal structures of the complexes of human Rap1a and the RBD of the Ser/Thr protein kinase Raf. According to results obtained with blast (http://www.ncbi.nlm.nih.gov/blast/bl2seq/wblast2.cgi) the sequence identity and sequence similarity between Rap (1C1Y) and Ras (1LFD) RBDs is 57% and 76%, respectively. For Raf and RalGDS RBDs, sequence alignment with blast/bl2seq is not possible. The alignment with ClustalW (http://www.ebi.ac.uk/clustalw) for Raf and RalGDS RBDs gives 18% sequence identity (14/77). We used 1C1Y in our study since Kiel et al. found a better correlation with the experimentally determined ΔG values for the mutants built from 1CLY than from 1GUA. For building mutant Ras-Raf complexes for which experimentally measured binding affinity is available,[29] mutations were introduced at 10 Ras residues (I21, H27, E31, D33, I36, E37, D38, S39, R41, V45) and 8 Raf residues (R59, N64, Q66, R67, T68, V69, K84, V88) (Fig. 2). The Ral–Rap complexes were built using 1GUA, the complex between RafRBD and the Rap K31E, E30D mutant, and 1LFD as templates. Rap from 1GUA and Ras from 1LFD were superimposed, and the RafRBD was replaced by RalGDS. Modelling was performed in the following way: E31 and D30 in Rap were mutated back to K and E, respectively, and the lowest energy rotamers of K and E were selected. The mutations were introduced at 4 Rap residues (P34, I36, D38, R41) and 12 RalGDS residues (R16, N23, N25, Y27, K28, S29, K44, D47, K48, H49, D52, E53). The mutations to A, as well as those from Y to F, were performed by simply deleting part of the side chain. F2

Water molecules included in the calculations were selected using InsightII.[48] The water molecules from the X-ray structures (1LFD and either 1GUA or 1CLY) close to the interacting proteins (within 6 Å of any of the proteins) were used for further optimization of the complexes. In the Ral-Ras complexes, 169 crystallographic water molecules were retained for the AB subunits and 199 for the CD subunits. The Rap-Ral and Raf–Ras complexes included 89 and 169 water molecules, respectively. The template for the Ral-Ras and Ral–Rap complexes contained 167 Ras residues, 87 RalGDS residues, GNP bound to Ras and Mg^{2+} coordinated with two GNP oxygens and oxygen atoms of Ras S17 and T35 amino acids. The template for the Ras–Raf complexes contained 167 Ras residues, 77 Raf residues, GNP bound to Ras and Mg^{2+} as well as Ca^{2+} at the surface of the Raf protein stabilized by the side chain oxygens of two glutamates (70 and 71) and the carbonyl oxygen of Gly69.

The nonpolar hydrogens were added using the tLeap module of AMBER8.0.[49] The polar hydrogen atoms of proteins and the bound water molecules were added using the program WHATIF.[50,51] It assigns histidines as singly or doubly protonated according to their hydrogen-bonding environment. Most of the histidines in RalGDS–Ras and Raf-Raf complexes are on the protein surface far from the binding interface. The closest to the binding interface are His27 in Ras and His49 in RalGDS which is buried. The ionization of these histidines is determined by local intramolecular contacts and not by whether the protein is free or in the complex.

The complexes with their experimental binding free energies are listed in Tables I and II of Supplementary

ID: 40408 Date: 4/2/07 Time: 12:15 Path: J:/Production/PROT/Vol00000/060260/3B2/C2PROT060260

J_ID: Z7E Customer A_ID: 21321 Cadmus Art: PROT21321 Date: 4-FEBRUARY-07 Stage: I Page: 4

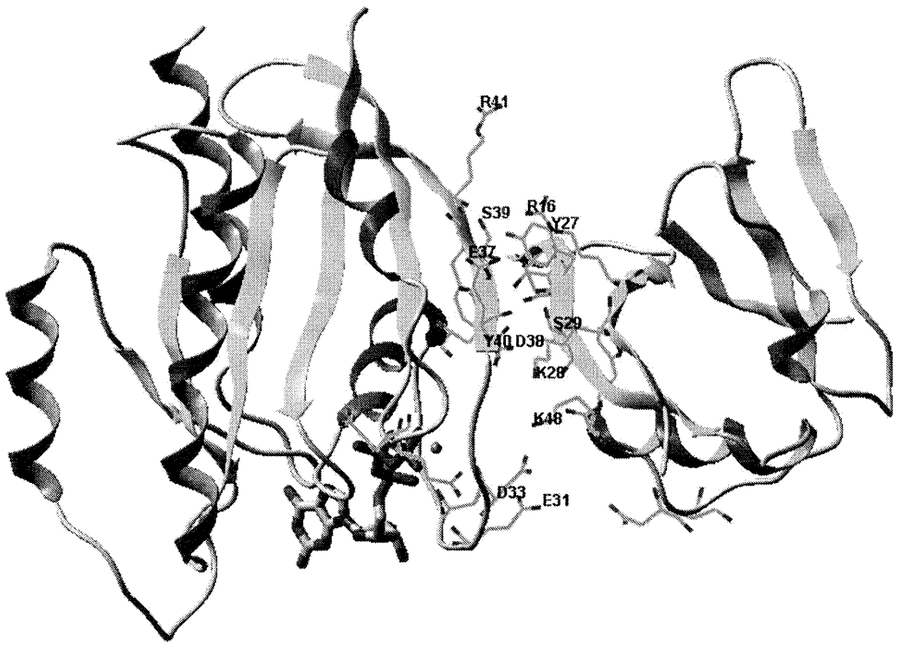

COLOR

Fig. 1. RalGDS–Ras complex (Ras on the left). The amino acids which were mutated (to A or F) are highlighted (thin sticks representation) and those that according to the COMBINE analysis are the most important for binding specificity are named. GNP is given in thick representation.

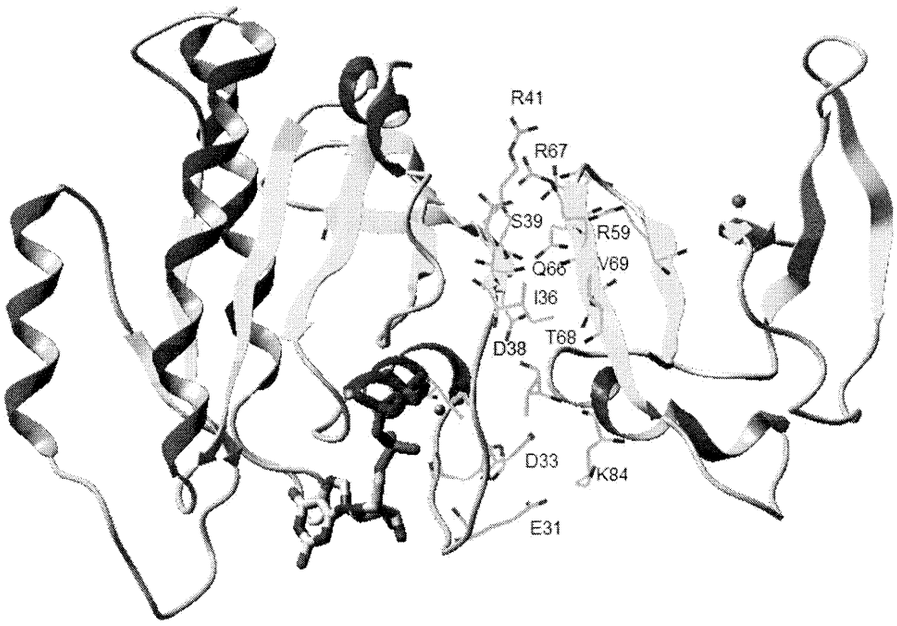

COLOR

Fig. 2. Raf–Ras complex, the amino acids which were mutated (to A or F) are highlighted (thin sticks representation) and those that according to the COMBINE analysis are the most important for binding specificity are named. GNP is given in thick representation.

Material. The binding free energies of the wild type complexes are −8.4 and −10.0 kcal/mol,[29] for the Ras–RalGDS and Ras–Raf complexes, respectively. According to the experimental results, the D47A, D52A, and E53A mutants of RalGDS (but no mutant of Raf) show higher binding affinities for the wild type Ras. The strongest binding for the Ras–RalGDS complexes was found to be −9 kcal/mol between the wild-type RalGDS and Ras: S39A mutant.

ID: 40408 Date: 4/2/07 Time: 12:15 Path: J:/Production/PROT/Vol00000/060260/3B2/C2PROT060260

J_ID: Z7E Customer A_ID: 21321 Cadmus Art: PROT21321 Date: 4-FEBRUARY-07 Stage: I Page: 5

The R41A mutant of Ras binds wild-type Raf (and its N64A mutant) stronger than the wild-type itself.

Energy minimization

The all atom force field of Duan et al. (2003), ff03,[49] was used for the proteins and water molecules. Parameters for GNP were derived using ANTECHAMBER and the Mg^{2+} radius (1.185 Å) was adopted from CHARMM. The parameters were adjusted to reproduce the conformation found in the unbound wild type Ras_GNP structure in the PDB (1CTQ). We found that the relative separation of Mg^{2+} and GNP in the crystal structure of the RalGDS–Ras complex 1LFD is about 1.9 Å larger than in the unbound wild type Ras_GNP structure. In the modeled wild type RalGDS–Ras complex, this difference is less than 1 Å. The tLeap module of AMBER8.0 was used to obtain the topology and coordinate files of each complex. Then, energy minimization of each complex was carried out using the Sander module of AMBER8.0 in two stages. In the first stage (500 steps), the protein nonhydrogen atoms were restrained to their starting positions by a harmonic potential with a force constant of 32 kcal/(mol Å^2) while the hydrogen atoms and the water molecules were unrestrained. In the second stage of 500 steps, no constraint was used at all. A nonbonded cutoff of 15.0 Å and a distance-dependent dielectric constant ($\varepsilon = r_{ij}$) were used throughout. In each stage, the first 100 steps were performed with the steepest descent algorithm and the rest of the steps were performed with the conjugate gradient method.

During the minimization, the backbone atoms of the mutated proteins did not show observable movement regarding their position in the crystal structure of the proteins, and only water molecules, particularly the additional interfacial water molecules, and some side chain atoms showed significant movements. The RMSD between the optimized and initial structure was never above the RMSD between the two complexes in the asymmetric crystal unit.

Electrostatic Binding Free Energy Calculations

To investigate the electrostatic contributions to the proteins' desolvation upon complex formation, we performed continuum electrostatic calculations using the program UHBD6.1.[52] The electrostatic contribution to the desolvation energy of each protein is defined as the loss of the electrostatic interaction between the solvent and a protein upon binding, as calculated by the two-step procedure described by Perez et al.[53] In the first step, the electrostatic interactions within each of the proteins and the surrounding solvent in the absence of the other protein is calculated, and in the second the electrostatic interactions between each of the proteins and the surrounding solvent with the bound pair-protein without partial charges. The electrostatic desolvation energy ($\Delta G_{ele}^{desol\_ras}$ or $\Delta G_{ele}^{desol\_ral}$) is given as the difference between the electrostatic energies computed from these two steps. The Poisson–Boltzmann equation was solved using the finite difference method implemented in UHBD6.1. The interior dielectric constant of the protein was set to two and the solvent dielectric constant was set to 78 with an ionic strength of 50 mM and ionic radius of 1.5 Å. The coarse grid spacing was set to 0.80 Å and the fine grid spacing was set to 0.35 Å. The dielectric boundary was defined as the van der Waals surface. Both the coarse grid and the fine grid were dimensioned to 110 × 110 × 110 with the center on the position of the Cα atom of D38/Ras in the case of RalGDS–Ras(p) complexes, and with the center on the position of the N atom of D57/Ras in the case of Raf–Ras complexes. The two grid centers are 5 Å apart, reflecting the difference in size and position of the two effectors. The coarse grid enclosed the whole protein complex while the fine grid enclosed the interface, including all residues mutated.

Before doing the UHBD calculations, the minimized structures of all the complexes were superposed with the minimized structure of the wild type complex to ensure the same reference coordinates. Then, a separate program[47] was used to convert the superposed structures of the complexes to qcd format files for input to UHBD 6.1, with all water molecules removed.

In both steps one and two described earlier, the structures of the Ras proteins and their effectors as found in the bound conformation in the complexes were used.

Interaction Energy Decomposition

The energy terms used to define binding free energy (ΔG) [Eq. (1)] are the electrostatic desolvation energies of Ras-GppNHp (Ras) or Rap-GppNHp (Rap) and its effector, either RalGDS-RBD (RalGDS) or Raf-RBD (Raf), upon binding, $\Delta G_{ele}^{desol\_ras}$ and $\Delta G_{ele}^{desol\_effector}$ respectively, and the pair wise electrostatic, E_i^{ele}, and van der Waals, E_i^{vdw}, interaction energies in energy minimized structures of the complexes. Interactions between each Ras(p) and each either RalGDS or Raf residue, as well as between GNP and Mg^{2+} and each effector residue, were determined using the ANAL module of AMBER8.0. A separate code was written to prepare input for GOLPE by extracting the intermolecular electrostatic and van der Waals energy terms, as well as the electrostatic interaction between the partner proteins and their electrostatic desolvation energies calculated with UHBD. For each RalGDS–Ras(p) and Raf–Ras complex, 29,409 (= 169 × 87 × 2 + 3) and 26,367 (= 169 × 78 × 2 + 3) energy descriptors, respectively, were generated. The binding free energy, ΔG, was estimated as a weighted linear sum of these energy descriptors as given in Eq. (2).

$$\Delta G = w_{ras}^{desol}\Delta G_{ele}^{desol\_ras} + w_{effector}^{desol}\Delta G_{ele}^{desol\_effector} + \sum_i w_i^{vdw}E_i^{vdw} + \sum_i w_i^{ele}E_i^{ele} + C \quad (2)$$

Chemometric Analysis

The GOLPE4.5.1 program[54] was used to carry out the chemometric analysis, that is to obtain the weights

ID: 40408 Date: 4/2/07 Time: 12:15 Path: J:/Production/PROT/Vol00000/060260/3B2/C2PROT060260

J_ID: Z7E Customer A_ID: 21321 Cadmus Art: PROT21321 Date: 4-FEBRUARY-07 Stage: I Page: 6

in Eq. (2), namely the parameters: $w_{\text{Ras}}^{\text{desol}}$, $w_{\text{effector}}^{\text{desol}}$, w_i^{vdw}, w_i^{ele}, and C. Matrices of the size 54 × 29,409, 22 × 29,409, and 46 × 29,367 were constructed. Each row represents a protein–protein complex described with 29,409 or 29,367 energy terms, the so-called X-variables (Coulombic energy terms, Lennard-Jones energy terms, two desolvation energies, and electrostatic interaction) and the binding free energy (Y-variable).

To reduce the size of the matrix, the X-variables of small absolute value and those showing little variation among the complexes, less than 0.01 kcal/mol, were neglected. To investigate the distribution of the complexes in the energy space defined by these X-variables, a principal component analysis (PCA) was performed. The distances between complexes were measured by the PCA scores. Then, the X-variables were correlated with the Y-variable by PLS analysis to yield initial PLS models of varying dimensionality. To remove the noisy variables and improve the predictive abilities of the PLS models, an X-variable selection procedure consisting of a D-optimal preselection and a fractional factorial design (FFD) was performed. The D-optimal preselection removed nearly half of the X-variables without affecting model quality, and the FFD further removed a few X-variables while retaining uncertain variables. Approximately equal numbers (ca. 10) of the Ras protein residues and its effector residues are included in the interaction energy terms of the final models.

To further evaluate the robustness of the data and the models, we randomly selected three test sets, each containing 41 complexes for training and 12 complexes for external prediction in the case of RalGDS–Ras complexes. In the case of Raf–Ras complexes, we selected three test sets, each containing the same 19 single mutant complexes and 6 different, randomly selected, double mutant complexes for training and the remaining sets of 21 double mutant complexes for external prediction.

RESULTS AND DISCUSSION

Energy Optimized Structures of Mutant Complexes

As in the study of Kiel et al.,[29] our investigation is based on the assumptions that single point mutations do not induce major conformational changes in the proteins (Raf, RalGDS, Ras and Rap) and that the conformations of the proteins do not change significantly upon complexation. However, to increase the robustness of the 3D QSAR model, we, instead of using a single structure, used values averaged from two different structures prepared using the two complexes found in the asymmetric unit of the crystal structure (1LFD). The RMSD between the initial and the geometry optimized structure of a mutant was always less than the RMSD between these two complexes (0.7 Å for backbone atoms).

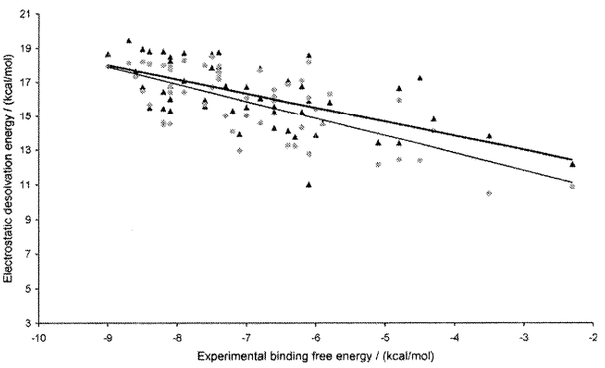

Fig. 3. Linear correlations between the RalGDS–Ras experimental binding free energy ΔG_{exp} and the computed continuum electrostatics desolvation energies of Ras (gray dots, thin line) and RalGDS (black triangles, thick line).

Computed Electrostatic Binding Free Energy Components Correlate With Experimental Binding Free Energies

The calculated $\Delta G_{\text{ele}}^{\text{desol\_ras}}$ and $\Delta G_{\text{ele}}^{\text{desol\_ral}}$ values from the Poisson–Boltzmann electrostatics calculations are listed in Table I of Supplementary Material along with the values of the experimental binding free energy, ΔG_{exp}. It should be noted that the values reported were computed with a dielectric boundary defined by the protein van der Waals surface. Calculations performed for barnase-barstar complexes[47] revealed that defining the boundary by the solvent accessible surface area leads to greater desolvation costs and a poorer correlation of electrostatic binding free energy with experimental binding affinities.

The linear correlation coefficients between the Ras–RalGDS experimental binding free energy ΔG_{exp}, and the electrostatic desolvation energy of Ras $\Delta G_{\text{ele}}^{\text{desol\_ras}}$ and the desolvation of RalGDS $\Delta G_{\text{ele}}^{\text{desol\_ral}}$ are −0.69 and −0.61, respectively (Fig. 3). For Ras–Raf complexes, a correlation of −0.46 and −0.62 for Ras and Raf, respectively was obtained, the correlation being weaker in these complexes for Ras. Similarly to the results obtained for barnase-barstar complexes,[47] the unfavorable desolvation energies of both the Ras protein and its effectors are negatively correlated with the experimental binding free energy, *i.e.* the tightest complexes have the highest desolvation penalties. Apparently, the favorable electrostatic interaction between the partner proteins balances out the unfavorable desolvation effects. The correlation coefficient between the electrostatic interaction energy, calculated by UHBD, and the measured binding free energy is 0.72 for the RalGDS–Ras, and 0.63 for the Raf–Ras complexes. The correlations between the total electrostatic contribution to the binding free energies, calculated by UHBD ($\Delta G_{\text{ele}}^{\text{desol\_ras}} + \Delta G_{\text{ele}}^{\text{desol\_effector}} + E_{\text{int}}^{\text{ele}}$), and the binding free energies determined by isothermal titration calorimetry, are about 0.67 for both data sets (Fig. 4).

ID: 40408 Date: 4/2/07 Time: 12:15 Path: J:/Production/PROT/Vol00000/060260/3B2/C2PROT060260

J_ID: Z7E Customer A_ID: 21321 Cadmus Art: PROT21321 Date: 4-FEBRUARY-07 Stage: I Page: 7

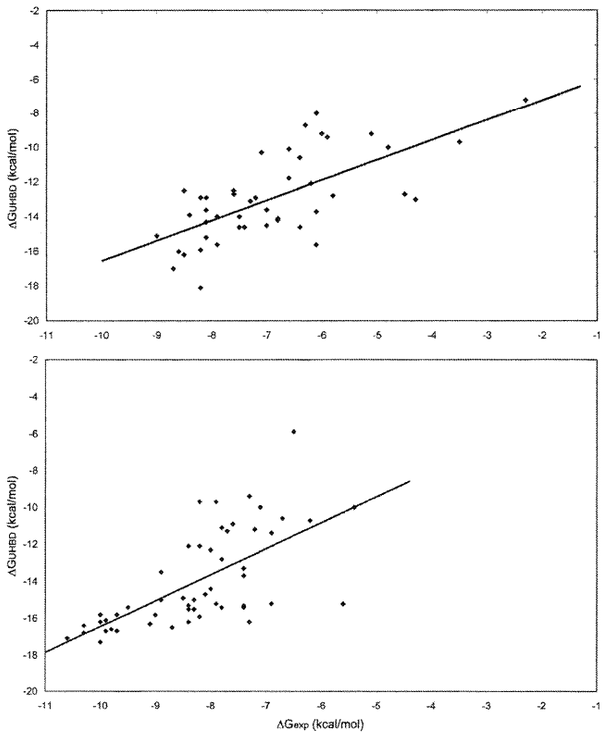

Fig. 4. Linear correlation between the experimental binding free energy ΔG_{exp} and the electrostatic contribution to the binding free energy (computed by UHBD), for RalGDS–Ras (top), and Raf–Ras complexes (bottom).

Principle Component Analysis for RalGDS–Ras Complexes

The score plot of the first two principal components (PC1 and PC2) for the Ras–Raf complexes is shown in Figure 5. The majority of the complexes is grouped in the lower left quadrant. Exceptions are the complexes with the E37A mutation in Ras which are all grouped in the upper right quadrant and have the largest positive PC1; the complexes with the D33A mutation of Ras, all grouped in the upper left quadrant; and the complexes with the K48A mutation in RalGDS also grouped in the upper left quadrant and having the largest negative PC1 and the largest positive PC2. The complexes with the D38A mutation in Ras are slightly dislocated from the largest group of complexes (grouped in the lower left quadrant) in the direction of the zero value of PC2. The energy terms that dominate in the definition of PCs are desolvation energies and the following RalGDS–Ras electrostatic interactions: K48-D38, K28-D38, Y27-E37, R16-D38, S29-D38, K48-GNP and K48-Mg^{2+}. The principal component scores of the complexes in which one or both of these amino acid residues are mutated differ significantly from those in the complexes in which they are not mutated. As a consequence, the particular mutant complexes form groups that are distant from each other and from the rest of the complexes in the score plot (Fig. 5).

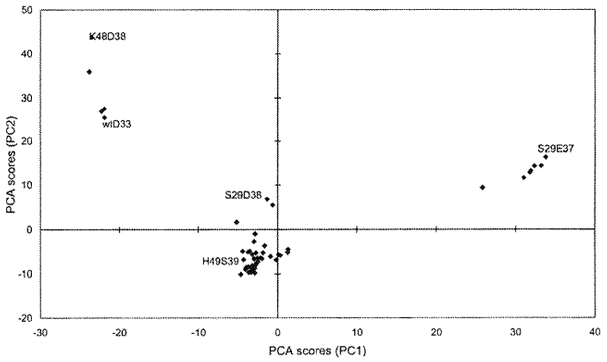

Fig. 5. Score plot of the first (PC1) and second (PC2) principal components of the energy terms for 53 RalGDS–Ras complexes. The representative complexes used to build the 5-object COMBINE model are named.

The principal component analysis highlights the energy terms important for the specificity of formation of RalGDS–Ras complexes.

The PC analysis served as a guide for identifying the most representative complexes to include in a minimal representative data set for building a QSAR model by PLS. The correlation between the dominating interactions and the binding affinities will be illustrated by the following PLS analysis.

PLS Analysis for RalGDS–Ras Complexes

The statistical parameters of the final COMBINE PLS models derived for the RalGDS–Ras complexes are given in Table I. The optimal dimensionality, before the variable selection procedure (models not shown in Table I), was determined as two latent variables because the model quality (as measured by fitting (R^2 and SDEC) and cross-validation (Q^2 and SDEP) parameters) did not increase significantly by adding more latent variables (Fig. 1 of Supplement Material). After the variable selection dimensionality of the model decreased from 2 to 1 LV, see Table I. Exclusion of the complex between RalGDS and RasY40A, WTY40A, resulted in significant improvement of the model performance.

The predicted binding free energies are listed in Table I of Supplementary Material. In leave-one-out cross-validation, 50 of the 53 complexes were predicted with an error less than 1.5 kcal/mol. The additional QSAR models were derived using either AMBER, or UHBD energy terms only. Both these models are predictive (Q^2 above 0.4). The three 41-complex training sets were randomly selected and PLS models were built. The mean external SDEP values determined for the remaining 12 complexes is 1.02 ± 0.40 kcal/mol (Table I). These SDEP values are mostly close to the SDEP value obtained in leave-one-out cross-validation, indicating robustness of the model.

The complexes with RalGDS:Y27 mutated to Ala were relatively poorly predicted by all these models (with $\Delta\Delta G$ being about 1–2 kcal/mol, see Table I, supplementary material). Tyr 27 in RalGDS is apparently stabilized by side-chain interactions with Arg 16 in the same protein

ID: 40408 Date: 4/2/07 Time: 12:15 Path: J:/Production/PROT/Vol00000/060260/3B2/C2PROT060260

J_ID: Z7E Customer A_ID: 21321 Cadmus Art: PROT21321 Date: 4-FEBRUARY-07 Stage: I Page: 8

TABLE I. Predictive Performance of the Final COMBINE Models Derived for Different Sets of Wild-Type and Mutant RalGDS-Ras Complexes

No. of complexes in the training set	X-variables	LV	R^2	SDEC (kcal/mol)	Q^2	SDEP internal (kcal/mol)	SDEP external for data averaged	SDEP external for AB unit only
54	All	1	0.60	0.89	0.54	0.96	–	–
53[a]	All	1	0.66	0.80	0.60	0.88		
53	AMBER	2	0.72	0.73	0.62	0.85		
53	UHBD	3	0.56	0.92	0.49	0.99		
41[b] (3x)	All	1	0.68 ± 0.08	0.72 ± 0.14	0.59± 0.11	0.81 ± 0.17	1.02 ± 0.40	1.06 ± 0.21
5 (PC based)	All	3	0.99	0.02	0.71	1.06	1.13	1.07

[a]The binding free energies predicted by this model are given in the last column of Table I of Supplement Meterial.
[b]The mean values of three models derived for the three randomly selected 12-object test data sets are given.

(the distance between the hydroxyl O and NH_2 is less than 3 Å). The mutation of Y27 to Ala abolishes this stabilization, so this might influence the protein stability, and accordingly reduce the binding affinity. Since, our COMBINE models do not consider the change in protein stability; the predicted binding affinities are more favorable than the measured ones.

To examine the applicability of the COMBINE procedure for planning efficient experiments to alter binding by mutation, we prepared a 3D QSAR model using only five complexes selected on the basis of the PC analysis score plot such that we selected one object from each of the five distinct groups. The following objects were selected: K48AD38A, WTD33A, S29AE37A, S29AD38A, H49AS39A. In this way, the training set spanned the majority of the PC space. The model derived with these five objects has good predictive performance: before FFD, the Q^2 value is 0.52, and SDEP for the other 48 (test) complexes is 1.17, and after FFD the Q^2 value is 0.71, and SDEP for the other 48 complexes 1.13, (Table I). The external prediction quality of this model is similar to the external prediction quality for the models derived using a training set of 41 randomly selected complexes.

To investigate which of the energy terms were highly weighted in the COMBINE model, we listed the thirty terms with the highest coefficients. The RalGDS amino acid residues that appear in these terms are I15, R16, D22, N23, G24, N25, M26, Y27, K28, S29, I30, R43, K44, A45, D47, K48, H49, N50, D52, E53, and D90. The Ras amino acid residues that appear in these terms are K5, K16, N25, E31, D33, P34, T35, I36, E37, D38, S39, Y40, R41, D54, L56, D57, N61, E63, R68, and GNP and the Mg^{2+} ion. The list includes all the RalGDS and Ras hotspot residues given by Kiel et al.[28] The top 10 PLS coefficients of the selected X-variables (energy terms), namely the weight parameters $w_{\text{Ras}}^{\text{desol}}$, $w_{\text{Ral}}^{\text{desol}}$, w_i^{vdw} and w_i^{ele} in Eq. (1), are plotted in Fig. 6. F6

By multiplying these weights with the corresponding energies, we obtain the contribution of the energy terms to the computed binding affinity. However, some of these terms make contributions that are opposite to their expected contribution. For example, increasing the protein electrostatic desolvation energy leads to more favorable computed binding affinity. This is because increased electrostatic desolvation energy correlates with increased favorable electrostatic interactions (see previous section). The model derived using AMBER energy terms is the most appropriate to investigate the influence of the certain pairwise intermolecular amino acid residue interactions on the binding free energy. For this purpose we multiplied weights above 0.01 with the corresponding energies calculated for the complex between wild type proteins. The most stabilizing interactions are those between Ras:D38 and Ral residues K28 and K48 (−1.65, and −0.85 kcal/mol, respectively) and the Ras:E37-Ral:Y27 interaction (−1.46 kcal/mol, Fig. 7). Interactions with unfavorable contributions to the binding affinity make contributions with much lower magnitude. The highest are Ras:E31-Ral:D52, Ras:E31-Ral:D47, and Ras:S39-Ral:Y27 interactions, all below 0.07 kcal/mol. F7

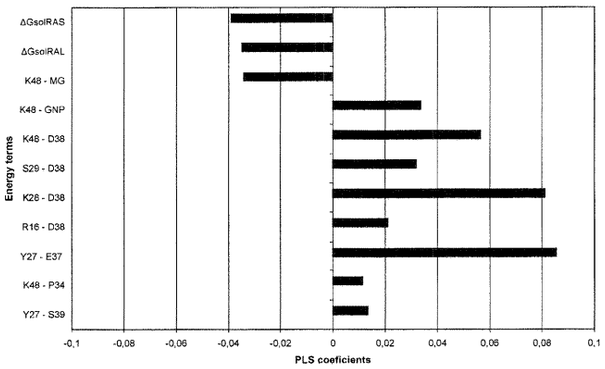

Fig. 6. The highest weighted energy terms (Ral_AA-Ras_AA) in the 3D QSAR model derived by COMBINE analysis for 53 wild-type and mutant Ras–RalGDS complexes. The 1st energy term, Y27-S39, is Van der Waals and the other terms are electrostatic interactions.

Beside models for RalGDS–Ras complexes, we also derived a model with a training set of 22 RalGDS-Rap complexes. The model based on UHBD desolvation energies and AMBER energy interaction terms has R^2 and Q^2 values of 0.62 and 0.48, respectively, and SDEC and SDEP values of 0.72 and 0.85 kcal/mol, respectively. The COMBINE model, even when trained with a small number of carefully selected mutants, predicts the RalGDS–Ras binding affinity fairly well. However, it should be

ID: 40408 Date: 4/2/07 Time: 12:16 Path: J:/Production/PROT/Vol00000/060260/3B2/C2PROT060260

J_ID: Z7E Customer A_ID: 21321 Cadmus Art: PROT21321 Date: 4-FEBRUARY-07 Stage: I Page: 9

born in mind that the COMBINE model is system-specific and the good prediction of the Ras–RalGDS binding affinity is not a guarantee that the binding affinities between the other proteins from the Ras family and their effectors (for example RalGDS-Rap and Raf–Ras) will be correctly predicted. Robustness of the models derived for the RalGDS–Ras complexes (Table I) was tested in a way that they were used to predict binding affinities for RalGDS-Rap complexes. The SDEPs determined for the 22 RalGDS-Rap complexes were between two and three. The best prediction of the RalGDS-Rap binding affinities was obtained with the model trained with five objects selected on the basis of PC analysis (SDEP = 2.24), followed by predictions with the UHBD and AMBER models trained with the 53-object data set. After correction for the difference in average energy of the datasets, $\sqrt{\sum_i^N (y_{\exp}^i + (\overline{\Delta G_t} - \overline{\Delta G_M}) - (y_{calc}^i)^2 / n}$, where $\overline{\Delta G_t}$ and $\overline{\Delta G_m}$ are the mean free binding energies of the test (RalGDS-Rap) and the training (Ras–RalGDS) sets, SDEP improves. The SDEPs determined for the test set of 22 RalGDS-Rap complexes with the 5-object (PC based), UHBD and AMBER models (Table I) are 1.29, 1.24, and 1.21 kcal/mol, respectively.

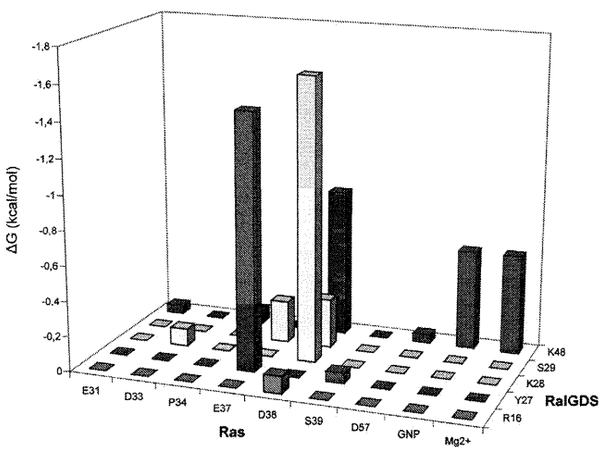

Fig. 7. The favorable contributions (< −0.05 kcal/mol) to the binding free energy of the wild type RalGDS–Ras complexes (AMBER model, see Table 1). [Color figure can be viewed in the online issue, which is available at www.interscience.wiley.com.]

PCA Analysis for Ras–Raf Complexes

In the score plot of the first two principal components (PC1 and PC2) for the Ras–Raf complexes (Fig. 2 of Supplementary Materials), the majority of the complexes, as in the PC analysis for Ras–RalGDS, is grouped in the lower left quadrant. Exceptions are the complexes with the E37A mutation in Ras which are all grouped in the upper quadrants and have the largest positive PC2; one of them, the K84AE37A complex, is positioned alone in the upper right quadrant. The complexes with either the Raf:K84A or Ras:E31A mutation are grouped in the lower right quadrant and have the largest negative PC2 and the largest positive PC1.

The energy terms that dominate in the definition of PCs are the electrostatic interactions between Ras:E37 and Raf residues R59, N64 and T68, those between Ras:D38 and Raf residues T68 and K84, and the GNP-Raf:K84 interaction. In the K84E37 (K84AE37A) mutant, most of these interactions are abolished, so it has an isolated position in the loading plot. This is in agreement with the experimental results according to which the binding free energy for this mutant is 3.5 kcal/mol less favorable than the binding free energy for the wild type protein complex (−6.5 *vs* −10 kcal/mol).

PLS Analysis for Raf–Ras Complexes

3D QSAR models were derived for a training set of 46 Raf–Ras complexes built using the coordinates of the complex in PDB file 1CLY to model the Raf mutants and the B subunit from the PDB file 1LFD to model the Ras mutants. The models are of good predictive performance, see Table II. COMBINE models determined for three 25-object training sets, randomly extracted from the 46-object data set, were used to predict the binding affinities of the complexes in the remaining 21-object data sets. The mean external SDEP calculated from these three models is 1.11 ± 0.07 kcal/mol (the experimental binding free energies span about 5 kcal/mol, from −10.6 to −5.4). The complexes with the I36A Ras mutation are poorly predicted by all models, with R59I36 being an outlier. To examine the influence of slight variation in geometry on the COMBINE model performance, two additional 3D QSAR models were derived: (a) for the set of further optimized complexes, and (b) for the set of data averaged over the complexes obtained using Ras from two different asymmetric units of 1LFD (B and D).

TABLE II. Predictive Performance of the COMBINE Models Derived for Raf–Ras Complexes

Number of complexes	X-variables	LV	R^2	SDEC (kcal/mol)	Q^2	SDEP Internal (kcal/mol)	SDEP_AB external[a] (kcal/mol)
46	All	5	0.85	0.48	0.69	0.68	–
46	AMBER	5	0.81	0.54	0.64	0.74	–
46	UHBD	3	0.48	0.89	0.40	0.96	–
5 PCA based	All	2	0.96	0.26	0.73	0.66	1.20 (41) 1.06 (40)[b]

[a]Number of objects in the test data set is given in brackets.
[b]R59I36 removed from the external data set.

ID: 40408 Date: 4/2/07 Time: 12:16 Path: J:/Production/PROT/Vol00000/060260/3B2/C2PROT060260

J_ID: Z7E Customer A_ID: 21321 Cadmus Art: PROT21321 Date: 4-FEBRUARY-07 Stage: I Page: 10

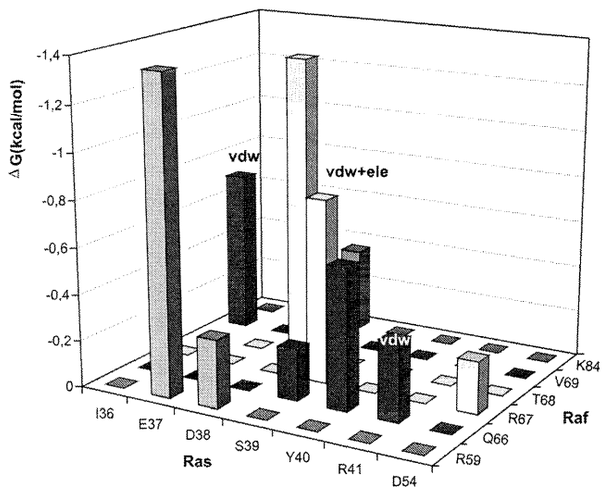

Fig. 8. The favorable contributions (greater than 0.2 kcal/mol in magnitude) to the binding free energy of the wild type Raf–Ras complexes (3D QSAR COMBINE-AMBER model trained with 46 wild-type and mutant Ras-Raf complexes). [Color figure can be viewed in the online issue, which is available at www.interscience.wiley.com.]

The averaging did not significantly influence the predictive performance of the model, while reoptimization slightly reduced the model performance (data given in Table III of Supplementary Materials).

The models derived using either only the UHBD or only AMBER energy terms are also listed in Table II. Both are predictive, but the latter has better performance. Unlike the models derived for the RalGDS–Ras complexes, the 'AMBER-only' model has slightly lower predictive performance than the model obtained using both AMBER and UHBD variables.

To determine which of the highly weighted pairwise, intermolecular energy terms are the most important for the free energy in a strongly binding complex, we multiplied weights in the COMBINE model ($R^2 = 0.85$, $Q^2 = 0.69$) with the corresponding energy terms calculated by AMBER for the wild type Ras–Raf complex. The greatest contributions to the binding free energy are shown in Figure 8. It is interesting that the Van der Waals interactions play a more significant role in this model than in the model derived for the RalGDS–Ras complexes. The highest Van der Waals interaction energy term favorably contributing to the binding free energy is that between Ras:I36 and Raf-V69. Beside the amino acid residues that were mutated in the study, a few nonmutated sites, namely Ras:Y40 and Raf residues T57 and R89, appear as important. Ras residue Y40 strongly interacts with Raf:Q66 ($E_{AMBER} = -3.2$ kcal/mol) and in this way stabilizes the complex (ΔG_i = ca −0.6 kcal/mol). The contribution of the unfavorable pairwise energy terms is higher in the Ras–Raf COMBINE models than in the Ras–RalGDS models. The most destabilizing energy terms are the electrostatic interactions between Ras:S39-Raf:R89 and Ras:R41-Raf:N64 with 1.4 and 0.7 kcal/mol, respectively. Both these interaction are attractive, but because of negative weights unfavorably contribute to the predicted binding free energy. Possible explanation is that desolvation cost of Raf residues N64 and R89 is not compensated with the attractive electrostatic interactions with Ras.

To improve the favorable Ras:36-Raf:57 interaction, we computationally mutated Raf:T57 to tyrosine, resulting in T57Y being expected to bind as well or slightly better than WT; according to the COMBINE model ΔG is −9.2 and −9.4 kcal/mol for the wild type proteins and T57YWT, respectively Besides the Ras:I36-Raf:Y57 interaction (ca −0.15 kcal/mol), some other favorable contributions to the binding free energy are computed to improve slightly upon this mutation.

The COMBINE Models for Cross Prediction of Binding Affinities of RalGDS–Ras and Raf–Ras Complexes (the Reduced COMBINE Models)

The number of X variables, as defined in Eq. (2), in the COMBINE models for RalGDS–Ras(p) and Raf–Ras complexes differ because of the different sizes of the effector proteins, and a COMBINE model derived for the one set of these Ras-effector complexes cannot be used directly to predict binding affinity at the other. However, the reduced, UHBD model consisting only of the proteins desolvation energy (ΔG_{Ras}, ΔG_{Raf},), the first two terms in Eq. (2), and the electrostatic interaction between them, E^{el}, can be used for the 'cross prediction' between the sets of different protein complexes. Using the 'UHBD_3' model (Table II) derived for the Raf–Ras set of complexes, we predicted binding affinities for the RalGDS–Ras and RalGDS-Rap mutants. The SDEPs obtained with the model that accounts for difference in the average binding free energy of the Ras–Raf and Ras–RalGDS complexes are 1.20 and 1.15 kcal/mol for Ras–RalGDS and Rap-RalGDS complexes, respectively. Beside this, the models including the interaction energy terms were also adjusted to be used for cross validation of two different sets of complexes: RalGDS–Ras(p) and Raf–Ras. For this purpose, the whole effector was treated as one group interacting with each amino acid residue of Ras protein. In this way, we derived two different COMBINE models, one based on AMBER Van der Waals and electrostatic interaction energies, and the other based on UHBD electrostatic interaction energies. Beside the Ras-residue based interaction energies, the desolvation energy terms and the total PB electrostatic interaction energy were also included. The number of X-variables used to derive these models is 341 (169 × 2 + 3), and 171 (169 + 2), respectively. The UHBD_171 model is more robust than AMBER_341 and has better external predictive performance (Table III). For 39 out of 53 RalGDS–Ras complexes, the binding affinity is predicted by the UHBD_171 model with an error less than 1.5 kcal/mol (Fig. 9). The correlation between experimental and predicted binding affinities for RalGDS–Ras complexes is about 0.61. Binding affinities for complexes with RalGDS-Y40 mutated to either alanine or phenylalanine

ID: 40408 Date: 4/2/07 Time: 12:16 Path: J:/Production/PROT/Vol00000/060260/3B2/C2PROT060260

J_ID: Z7E Customer A_ID: 21321 Cadmus Art: PROT21321 Date: 4-FEBRUARY-07 Stage: I Page: 11

TABLE III. Predictive Performance of the COMBINE Models, with the Effector Treated as One Group, Derived for 46- Raf–Ras Complexes

No. of LVs	No. of X-variables	R^2	SDEC (kcal/mol)	Q^2	SDEP Internal (kcal/mol)	SDEP External[a] (kcal/mol)	SDEP External[b] (kcal/mol)
2	341	0.98	0.19	0.62	0.79	1.01	1.23
3	171	0.54	0.83	0.41	0.94	0.91	

[a]External prediction for 53- RalGDS-Ras complex data set.
[b]External prediction for 22- RalGDS-Rap complex data set.
In both cases, the correction for the difference in average energies of the datasets is applied.

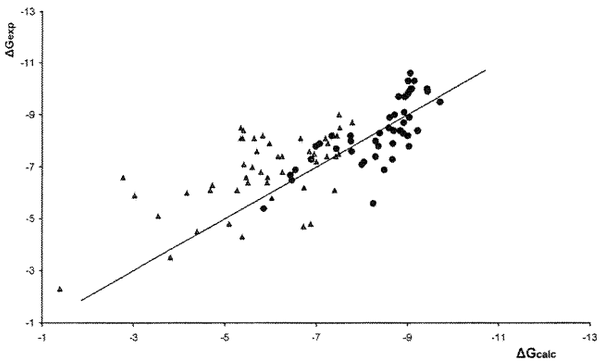

Fig. 9. UHBD 171 model - plot of experimental versus calculated binding affinities for Raf–Ras (dots) and RalGDS–Ras (triangles) complexes, respectively. The binding affinities for RalGDS–Ras are calculated using the COMBINE model trained with data on Raf–Ras only.

and RalGDS–RasY27A are poorly predicted, but these complexes were poorly predicted even with the COMBINE model derived for the RalGDS–Ras complexes. The electrostatic interactions between E37, D38, S39, Y40, D57 and GNP and Raf are the largest favorable contributions to the predicted binding affinity.

Recently Kiel et al.[55] made the M26K, D47K, E(D)54K RalGDS mutant and found that it binds to Ras 14-fold faster and 25-fold tighter compared with the wild-type. These three amino acid residues appear as interaction partners in the thirty highly weighted terms of the COMBINE model derived for the RalGDS–Ras complexes. However, their contribution to the binding free energy is much weaker than those of the RalGDS residues K28 and K48. The binding affinity for this complex predicted by the reduced UHBD based model is almost identical to the binding affinity predicted for the wild type RalGDS, that is −9.09 *vs* −9.07 kcal/mol. Apparently the COMBINE model predicted tight binding of the mutant, but not the large gain in binding affinity observed experimentally.

Possible Small Molecule Inhibitor Binding Sites

Trosset et al.[56] showed that it is possible to inhibit a protein–protein interaction by binding of a small molecule that tightly interacts with the hot spots at the protein interface. Such a hot spot position for the Ras would be in the vicinity of E37 and D38. However, a small molecule could be utilized to specifically inhibit binding of only one effector. According to the results of COMBINE analysis, we expect that a small molecule that would bind into the clefts between E31 and D33 and/or D33 and T35 should more significantly decrease the binding affinity of Ras to RalGDS than to Raf. Namely, the side chain oxygen of D33, E31 and T35, as well as the backbone oxygen of P34, tightly interact with Ral residues N50 and lysines 28 and 48 (highly weighted interactions in the COMBINE models derived for RalGDS–Ras complexes), while there are no such close interactions between Raf and these Ras residues (Raf is at this part of the Ras surface more distant from it than Ral). Another possible place for binding a small molecule with discriminating influence to Ras–Raf and Ras–RalGDS complexes might be in the vicinity of Y40, R41, and D54. At this part of the Ras surface, Raf is closer to it than Ral, and its residues N64, Q66, and R67 favorably interact with Ras residues Y40, R41, and D54.

Concluding Remarks

The electrostatic contributions to binding computed by solving the finite difference Poisson–Boltzman equation, with a van der Waals surface boundary definition, favor formation of complexes between Ras proteins (Ras and Rap) and their effectors (Raf and RalGDS).

The 3D QSAR models derived using COMBINE analysis are predictive not only for the complexes of the same Ras protein and its effector, *i.e.* for the mutants of the same partner proteins, but also for the sets of different Ras-effector protein complexes. The binding affinities of complexes with I36A and Y40A(F) Ras mutants were poorly predicted by all models. There are two possible explanations for this, one is changed (increased) stability of the mutant and the other is conformational change that improves complex formation. These effects could not be detected with the standard COMBINE approach.

The Ras amino acid residues that all, AMBER and UHBD based, COMBINE models for both datasets, RalGDs–Ras and Raf–Ras complexes, revealed as significantly stabilizing are E37, D38, and D57. Besides, in both data sets, an important stabilization is achieved by interaction between GNP and the effector protein. The other residues of the Ras protein that appear important for the models are K5, K16, E31, D33, P34, I36, S39, Y40, R41, and D54. The Raf–Ras complexes are specifically stabilized by the electrostatic interactions: Ras: Y40-Raf:Q66, Ras:S39-Raf:Q66, Ras:S39-Raf:R67, Ras: R41-Raf:Q66, and Ras:D54-Raf:R67; and the RalGDS–Ras complexes complexes are specifically stabilized by

ID: 40408 Date: 4/2/07 Time: 12:16 Path: J:/Production/PROT/Vol00000/060260/3B2/C2PROT060260

J_ID: Z7E Customer A_ID: 21321 Cadmus Art: PROT21321 Date: 4-FEBRUARY-07 Stage: I Page: 12

the electrostatic interactions between Ras residues E31 and P34 and Raf residue K48.

The present analysis enabled us to propose Ras amino acid residues important for discriminating binding of Raf and RalGDS. The results suggest that a small molecule that would specifically bind into the clefts between E31 and D33 and/or D33 and T35 could decrease the binding affinity of Ras to RalGDS more than to Raf. On the other hand a molecule bound in the vicinity of Y40, R41, and D54 could decrease the binding affinity of Ras to Raf more than to RalGDS.

The COMBINE models derived for only a few complexes selected according to the results of PC analysis successfully predicted binding affinities for the remaining, external set of complexes. This result allows us to point to the feasibility of this method for aiding experimental design. A number of *in silico* mutants accompanied by a PC analysis could be used as an initial base for selecting representative mutants to be analyzed experimentally. From the calculated energy interaction terms and the experimentally determined binding affinities for the selected mutants, the PLS model could be derived. Finally, binding affinities for the other, *in silico* prepared mutants would be predicted and those with the highest binding affinities would be selected for further experimental study. However, an important assumption of such an approach is that the mutations do not induce significant conformational changes in the protein.

The electrostatic components of ΔG calculated with UHBD correlate slightly better with the measured value than ΔG computed with the COMBINE model with the UHBD terms only (0.67 vs 0.61). However, ΔG values are by UHBD significantly overestimated, on average about 6 and 12 kcal/mol for RalGDS–Ras and Raf–Ras complexes datasets, respectively. On the other hand, binding affinities for 77% of the analyzed complexes are predicted by the COMBINE model with an error less than 1.5 kcal/mol. To estimate the relative binding affinity for a set of protein complexes standard Poisson–Boltzman electrostatic free energies can be computed, and this can be done in the absence of any experimental data on binding affinities. On the other hand, if experimental data are available for at least a few representatives, the COMBINE method may be useful. These two methods nicely complement one another since a reliable 3D structure of the complex is needed for both methods, and once the UHBD energies have been calculated, a PC and PLS (if affinity measurements are available) analysis can easily be performed and valuable information obtained.

If we compare COMBINE methods with more general methods to estimate binding affinity we can give arguments pro and contra. On the one hand, being system specific, it may capture features of the system important for binding affinity that are difficult to detect with a general scoring function. On the other hand, a drawback is that, being trained for a specific system, the accuracy of predictions falls off as complexes in the test set become more different from those in the training set. An advantage of the COMBINE method in comparison with most general scoring functions or methods to estimate binding affinity is that it explicitly suggests which amino acid residues should be targeted to adjust the binding affinity, either by mutation or by binding of a small molecule.

ACKNOWLEDGMENTS

We thank Prof. C. Herrmann for providing us data and for valuable discussion.

REFERENCES

1. Bourne HR, Sanders DA, McCormick F. The GTPase superfamily: a conserved switch for diverse cell functions. Nature 1990;348: 125–132.
2. Bourne HR, Sanders DA, McCormick F. The GTPase superfamily: a conserved switch for diverse cell functions. Nature 1991;349:117–127.
3. Rapp UR, Goldsborough MD, Mark GE, Bonner TI, Groffen J, Reynolds FH, Jr, Stephenson J. Structure and biological activity of v-raf, a unique oncogene transduced by a retrovirus. Proc Natl Acad Sci USA 1983;80:4218–4222.
4. Hamad NM, Elconin JE, Karnoub AE, Bai W, Rich JN, Abraham RT, Der CJ, Counter CM. Distinct requirements for Ras oncogenesis in human versus mouse cells. Genes Dev 2002;16: 2045–2057.
5. Singh A, Sowjanya AP, Ramakrishna G. The wild-type Ras: road ahead. FASEB J 2005;19:161–169.
6. Bos JL. All in the family? New insights and questions regarding interconnectivity of Ras, Rap and Ral. EMBO J 1998;17:6776–6782.
7. Wolthuis RM, Bos JL. Ras caught in another affair: the exchange factors for Ral. Curr Opin Genet Dev 1999;9:112–117.
8. Feig LA. The Ral GTPases: approaching their 15 minutes of fame. Trends Cell Biol 2003;13:419–425.
9. Hamad NM, Elconin JH, Karnoub AE, Bai W, Rich JN, Abraham RT, Der CJ, Counter CM. Distinct requirements for Ras oncogenesis in human versus mouse cells. Genes Dev 2002;16: 2045–2057.
10. Boettner B, Van Aelst L. The RASputin effect. Genes Dev 2002;16:2033–2038.
11. Agapova LS, Volodina JL, Chumakov PM, Kopnin BP. Activation of Ras-RalGDS pathway attenuates p53-independent DNA damage G2 checkpoint. J Biol Chem 2004;279:36382–36389.
12. Wittinghofer A, Herrmann C. Ras effector interactions, the problem of specificity. FEBS Lett 1995;369:52–56.
13. Nassar N, Horn G, Herrmann C, Scherer A, McCormick F, Wittinghofer A. The 2.2 Å crystal structure of the Ras-binding domain of the serine/threonine kinase c-Raf1 in complex with Rap1A and a GTP analogue. Nature 1995;375:554–560.
14. Nassar N, Horn G, Herrmann C, Block C, Janknecht R, Wittinghofer A. Ras/Rap effector specificity determined by charge reversal. Nat Struct Biol 1996;3:723–729.
15. Vetter IR, Linnemann T, Wohlgemuth S, Geyer M, Kalbitzer HR, Herrmann C, Wittinghofer A. Structural and biochemical analysis of Ras-effector signaling via RalGDS. FEBS Lett 1999;451:175–180.
16. Huang L, Hofer F, Martin GS, Kim SH. Structural basis for the interaction of Ras with RalGDS. Nat Struct Biol 1998;5:422–426.
17. Kigawa T, Yamaguchi-Nunokawa E, Kodama K, Matsuda T, Yabuki T, Matsuda N, Ishitani R, Nureki O, Yokoyama S. Selenomethionine incorporation into a protein by cell-free synthesis. J Struct Funct Genomics 2002;2:29–35.
18. Spoerner M, Wittinghofer A, Kalbitzer HR. Perturbation of the conformational equilibria in Ras by selective mutations as studied by 31P NMR spectroscopy. FEBS Lett 2004;17;578:305–310.
19. Emerson SD, Madison VS, Palermo RE, Waugh DS, Scheffler JE, Tsao KL, Kiefer SE, Liu SP, Fry DC. Solution structure of the Ras-binding domain of c-Raf-1 and identification of its Ras interaction surface. Biochemistry 1995;34:6911–6918.

ID: 40408 Date: 4/2/07 Time: 12:16 Path: J:/Production/PROT/Vol00000/060260/3B2/C2PROT060260

20. Huang L, Weng X, Hofer F, Martin GS, Kim SH. Three-dimensional structure of the Ras-interacting domain of RalGDS. Nat Struct Biol 1997;4:609–615.
21. Geyer M, Herrmann C, Wohlgemuth S, Wittinghofer A, Kalbitzer HR. Structure of the Ras-binding domain of RalGEF and implications for Ras binding and signaling. Nat Struct Biol 1997;4:694–699.
22. Walker EH, Perisic O, Ried C, Stephens L, Williams RL. Structural insights into phosphoinoside 3-kinase catalysis and signaling. Nature 1999;402:313–320.
23. Steiner G, Kremer W, Linnemann T, Herrmann C, Geyer M, Kalbitzer HR. Sequence-specific resonance assignment of the Ras-binding domain of AF6. J Biomol NMR 2000;18:73–74.
24. Gronwald W, Huber F, Grünewald P, Spörner M, Wohlgemuth S, Herrmann C, Kalbitzer HR. Solution structure of the Ras-binding domain of the protein kinase Byr2 from *Schizosaccharomyces pombe*. Structure 2001;9:1029–1041.
25. Scheffzeck K, Grünewald P, Wohlgemuth S, Kabsch W, Tu H, Wigler M, Wittinghofer A, Herrmann C. The Ras-Byr2RBD complex: structural basis for Ras effector recognition in yeast. Structure 2001;9:1043–1050.
26. Gohlke H, Kuhn LA, Case DA. Change in protein flexibility upon complex formation: analysis of Ras-Raf using molecular dynamics and a molecular framework approach. Proteins 2004;56:322–337.
27. Gohlke H, Case DA. Converging free energy estimates: MM-PB(GB)SA studies on the protein-protein complex Ras-Raf. J Comput Chem 2004;25:238–250.
28. Gohlke H, Kiel C, Case DA. Insights into protein-protein binding by binding free energy calculation and free energy decomposition for the Ras-Raf and Ras-RalGDS complexes. J Mol Biol 2003;330:891–913.
29. Kiel C, Serrano L, Herrmann C. A detailed thermodynamic analysis of Ras/effector complex interfaces. J Mol Biol 2004;340: 1039–1058.
30. Muegge I, Schweins T, Warshel A. Electrostatic contributions to protein-protein binding affinities: application to Rap/Raf interaction. Proteins 1998;30:407–423.
31. Sheinerman FB, Honig B. On the role of electrostatic interactions in the design of protein-protein interfaces. J Mol Biol 2002;318:161–177.
32. Kiel C, Wohlgemuth S, Rousseau F, Schymkowitz J, Ferkinghoff-Borg J, Wittinghofer F, Serrano L. Recognizing and defining true ras binding domains II: in silico prediction based on homology modelling and energy calculations. J Mol Biol 2005;348:759–775.
33. Madura JD, Briggs JM, Wade RC, Davis ME, Luty BA, Ilin A, Antosiewicz J, Gilson MK, Bagheri B, Scott LR, McCammon JA. Electrostatics and diffusion of molecules in solution: simulations with the university of Houston brownian dynamics program. Comput Phys Commun 1995;91:57–95.
34. Ortiz AR, Pisabarro MT, Gago F, Wade RC. Prediction of drug binding affinities by comparative binding energy analysis. J Med Chem 1995;38:2681–2691.
35. Ortiz AR, Pastor M, Palomer A, Cruciani G, Gago F, Wade RC. Reliability of comparative molecular field analysis models: effects of data scaling and variable selection using a set of human synovial fluid phospholipase A2 inhibitors. J Med Chem 1997;40:1136–1148.
36. Wade RC, Henrich S, Wang T. Using 3D protein structures to derive 3D-QSARs Drug Discovery Today: Technologies 2004;1: 241–246.
37. Wade RC. Derivation of QSARs using 3D structural models of protein-ligand complexes by COMBINE analysis. In: Holtje HD,Sippl W, editors. Rational approaches to drug design: 13th European symposium on quantitative structure-activity relationships. Barcelona: Prous Science SA; 2001. pp 23–28.
38. Pastor M, Gago F, Cruciani G.Comparative binding energy (COMBINE) analysis on a series of glycogen phosphorylase inhibitors: comparison with GRID/GOLPE methods. In: Gundertofter K,Jorgensen FS, editors. Molecular modeling and prediction of bioactivity. New York: Kluwer; 2000. pp 329–330.
39. Wang T, Wade RC. Comparative binding energy (COMBINE) analysis of influenza neuraminidase-inhibitor complexes. J Med Chem 2001;44:961–671.
40. Lozano JJ, Pastor M, Cruciani G, Gaedt K, Centeno NB, Gago F, Sanz F. 3D-QSAR methods on the basis of ligand receptor complexes. Application of COMBINE and GRID/GOLPE methodologies to a series of CYP1A2 ligands. J Comput Aided Mol Des 2000;14:341–353.
41. Tomic S, Kojic-Prodic B. A quantitative model for predicting enzyme enantioselectivity: application to burkholderia cepacia lipase and 3-(aryloxy)-1,2-propanediol derivatives. J Mol Graph Model 2002;21:241–252.
42. Tomić S, Bertoša B, Kojić-Prodić B, Kolosvary I. Stereoselectivity of Burkholderia cepacia lipase towards secondary alcohols: molecular modelling and 3D QSAR approach. Tetrahedron Asymmetry 2004;15:1163–1172.
43. Tomić S. Enantioselectivity of burkholderia cepacia lipase towards primary and secondary alcohols: molecular modelling and 3D QSAR analysis. In: Ford M, Livingstone D, Dearden J, vande Waterbeemd H, editors. Designing drugs and crop protectants: processes, problems and solutions. Oxford, UK: Blackwell; 2003. pp 326–328.
44. Wang T, Wade RC. Comparative binding energy (COMBINE) analysis of OppA-peptide complexes to relate structure to binding thermodynamics. J Med Chem 2002;45:4828–4837.
45. Tomic S, Nilsson L, Wade RC. Nuclear receptor-DNA binding specificity: a COMBINE and free-Wilson QSAR analysis. J Med Chem 2000;45:1780–1792.
46. Tomić S, Wade RC. COMBINE analysis of nuclear receptor-DNA binding specificity: comparison of two datasets. Croatica Chemica Acta 2001;74:295–314.
47. Wang T, Tomić S, Gabdoulline R, Wade RC. How optimal are the binding energetics of barnase and barstar? Biophys J 2004;12: 1563–1574.
48. InsightII version 2000. San Diego, CA: Accelrys, Inc.
49. Duan Y, Wu C, Chowdhury S, Lee MC, Xiong G, Zhang W, Yang R, Cieplak P, Luo R, Lee T, Caldwell J, Wang J, Kollman P. A point-charge force field for molecular mechanics simulations of proteins based on condensed-phase quantum mechanical calculations. J Comp Chem 2003;24:1999–1994.
50. Vriend G. WHAT IF: a molecular modelling and drug design program. J Mol Graph 1990;8:52–56
51. Hooft RW, Sander C, Vriend G. Positioning hydrogen atoms by optimizing hydrogen bond networks in protein structures. Proteins 1996;26:363–376.
52. Madura JD, Briggs JM, Wade RC, Davis ME, Luty BA, Ilin A, Antosiewicz J, Gilson MK, Bagheri B, Scott LR. Electrostatics and diffusion of molecules in solution: simulations with the university of Houston Brownian dynamics program. Comput Phys Commun 1995;91:57–95.
53. Perez C, Pastor M, Ortiz AR, Gago F. Comparative binding energy analysis of HIV-1 protease inhibitors: incorporation of solvent effects and validation as a powerful tool in receptor-based drug design. J Med Chem 1998;41:836–852.
54. Baroni M, Costantino G, Cruciani G, Riganelli D, Valigi R, Clementi S. Generating optimal linear PLS estimations (GOLPE): an advanced chemometric tool for handling 3D-QSAR problems. Quant Struct Act Rel 1993;12:9–20.
55. Kiel C, Selzer T, Shaul Y, Schreiber G, Herrmann C. Electrostatically optimized Ras-binding Ral guanine dissociation stimulator mutants increase the rate of association by stabilizing the encounter complex. PNAS 2004;101:9223–9228.
56. Trosset J-Y, Dalvit C, Knapp S, Fasolini M, Veronesi M, Mantegani S, Gianellini LM, Catana C, Sundström M, FW, Stouten PFW, Jürgen K, Moll JK. Inhibition of protein-protein interactions: the discovery of druglike β-catenin inhibitors by combining virtual and biophysical screening biophysical screening. Proteins 2006;64:60–67.